doi:10.1016/j.jmb.2011.07.006 J. Mol. Biol. (2011) 411, 1114–1127

Contents lists available at www.sciencedirect.com

Journal of Molecular Biology

journal homepage: http://ees.elsevier.com.jmb

The Structure of BRMS1 Nuclear Export Signal and SNX6 Interacting Region Reveals a Hexamer Formed by Antiparallel Coiled Coils

Mercedes Spínola-Amilibia[1], José Rivera[2], Miguel Ortiz-Lombardía[3], Antonio Romero[4], José L. Neira[5,6] and Jerónimo Bravo[1]*

[1]*Instituto de Biomedicina de Valencia (IBV-CSIC), C/ Jaime Roig 11, 46010 Valencia, Spain*
[2]*Centro Nacional de Investigaciones Cardiovasculares Carlos III, C/ Melchor Fernández Almagro 3, 28029 Madrid, Spain*
[3]*Architecture et Fonction des Macromolécules Biologiques, UMR6098, CNRS, Universités d'Aix-Marseille I and II, Case 932, 163 Avenue de Luminy, 13288 Marseille cedex 9, France*
[4]*Departamento de Biología Físico-Química, Centro de Investigaciones Biológicas, CSIC, C/ Ramiro de Maeztu 9, 28040 Madrid, Spain*
[5]*Instituto de Biología Molecular y Celular, Universidad Miguel Hernández, Edificio Torregaitán, 03202 Elche, Spain*
[6]*Instituto de Biocomputación y Física de Sistemas Complejos, Mariano Esquillor, Edificio I+D, 50018 Zaragoza, Spain*

Received 2 March 2011;
received in revised form
21 June 2011;
accepted 6 July 2011
Available online
18 July 2011

Edited by R. Huber

Keywords:
BRMS1;
metastasis suppressors;
coiled-coil domain;
X-ray diffraction;
structure

We present here the first structural report derived from breast cancer metastasis suppressor 1 (BRMS1), a member of the metastasis suppressor protein group, which, during recent years, have drawn much attention since they suppress metastasis without affecting the growth of the primary tumor. The relevance of the predicted N-terminal coiled coil on the molecular recognition of some of the BRMS1 partners, on its cellular localization and on the role of BRMS1 biological functions such as transcriptional repression prompted us to characterize its three-dimensional structure by X-ray crystallography.

The structure of BRMS1 N-terminal region reveals that residues 51–98 form an antiparallel coiled-coil motif and, also, that it has the capability of homo-oligomerizing in a hexameric conformation by forming a trimer of coiled-coil dimers. We have also performed hydrodynamic experiments that strongly supported the prevalence in solution of this quaternary structure for $BRMS1_{51–98}$.

This work explores the structural features of BRMS1 N-terminal region to help clarify the role of this area in the context of the full-length protein. Our crystallographic and biophysical results suggest that the biological function of BRMS1 may be affected by its ability to promote molecular clustering through its N-terminal coiled-coil region.

**Corresponding author.* Department of Genomics and Proteomics, Instituto de Biomedicina de Valencia (IBV-CSIC), C/ Jaime Roig 11, 46010 Valencia, Spain. E-mail address: jbravo@ibv.csic.es.

Abbreviations used: BRMS1, breast cancer metastasis suppressor 1; SNX6, sorting nexin 6; NES, nuclear export signal; NLS, nuclear localization signal; DOSY-NMR, diffusion-ordered spectroscopy nuclear magnetic resonance; DLS, dynamic light scattering; PDB, Protein Data Bank.

0022-2836/$ - see front matter

Introduction

Most human cancer deaths are caused by metastasis, a process involving several defined steps including detachment of cancer cells from a primary tumor, invasion of surrounding tissue, survival in the bloodstream, extravasation and colonization at distant organs.

Many genetic events are required to promote metastasis including several genes that show relative reduced expression levels in aggressive human tumors. Restoration of normal levels for some of these proteins in a metastatic tumor cell line results in a significant reduction of the metastatic behavior *in vivo* with no effect on primary tumor growth.[1] Little is known about the molecular events triggered by this family of genes known as metastasis suppressors. Nevertheless, its function seems to become increasingly relevant toward the final stages of the metastatic cascade.[2,3]

Breast cancer metastasis suppressor 1 (BRMS1), a member of this growing metastasis suppressor family, was identified by differential display and significantly reduced metastasis without affecting breast,[4] melanoma[5,6] or ovarian carcinoma[7] primary tumor growth.

BRMS1 transcriptional repression reduces metastasis and appears to be epigenetically regulated.[8,9] Molecular mechanisms of action for BRMS1 include restoration of cell–cell communication[10] and abrogation of phosphoinositide signalling.[11] It has been proposed that BRMS1 might induce all these changes by playing a role in transcription.[12–19] In fact, BRMS1 has the ability to form complexes with several proteins involved in the regulation of transcription.[18,20,21] Thus, BRMS1 can interact with a wide range of proteins in order to promote different effects on the metastatic cascade. Despite the wide biomedical interest, molecular characterization of BRMS1, including structural studies, remains largely elusive. Analysis of the BRMS1 primary structure predicts a mostly disordered protein showing a few putative motifs, including two nuclear localization signals (NLSs) in two predicted coiled-coil regions (Fig. 3d).

Coiled-coil regions have long been known as protein–protein interaction modules that can exert biologically relevant functions.[34,35] In fact, BRMS1 second predicted coiled-coil domain, including residues 130–187, is involved in interactions with AT-rich interactive domain 4A, part of the SIN3: histone deacetylase chromatin remodeling complex.[18] In addition, we have recently shown that BRMS1 N-terminal putative coiled coil interacts with a predicted coiled-coil region of sorting nexin 6 (SNX6) including residues 300–406, increasing BRMS1-dependent transcriptional repression.[21] Moreover, we have also shown that BRMS1 residues 74–91 have been identified as a functional nuclear export signal (NES).[33] Given that this predicted N-terminal coiled coil has an important role on the molecular recognition of some of the BRMS1 partners,[18,21] that it contains a sequence essential for its cytoplasmic localization,[33] and that it has also been related to important BRMS1 biological functions such as transcriptional repression, we wanted to characterize its three-dimensional structure. We had previously reported the crystallization of BRMS1 including residues 51–84[36] and now have solved the structure of the predicted BRMS1 coiled-coil region including residues 51–98 ($BRMS1_{51–98}$).

Structural characterization of this BRMS1 fragment reveals a trimer of antiparallel binary coiled coils. The crystal structure is in agreement with the solution oligomerization state determined by analytical ultracentrifugation and hydrodynamic experiments. This particular molecular arrangement might suggest the ability of BRMS1 to promote molecular clustering through its N-terminal coiled-coil region.

Results

$BRMS1_{51–98}$ crystal structure

Human BRMS1 N-terminal coiled-coil region (residues 51–98) was successfully expressed in *Escherichia coli* Rosetta(DE3)pLysS cells and purified by metal-chelating affinity chromatography followed by size-exclusion chromatography in a buffer containing 20 mM Tris–HCl (pH 7.5) and 50 mM NaCl. The elution volume of $BRMS1_{51–98}$ in the pre-calibrated gel-filtration column corresponded to an apparent molecular mass of ~32 kDa (data not shown). A major peak of protein, followed by absorption at 280 nm, was obtained at an elution volume of 160 mL. After analysis of more than 900 crystallization conditions and hit optimization, typical crystals grew with dimensions of 0.05 mm × 0.05 mm × 0.05 mm. Further improvement based mainly on the screening of different pH, precipitant concentration, temperature growing and protein:reservoir ratio volume led to 0.25 mm × 0.25 mm × 0.25 mm crystals after 3 days. Prior to data collection, crystals (Fig. 1a) were vitrified in the presence of paratone.

Diffraction data were collected and reduced to 1.9 Å. The data statistics of the X-ray diffraction experiments are shown in Table 1. Crystals are rhombohedral and belong to the *R*32 space group with unit cell dimensions, in the hexagonal setting, of $a = 60.4$ Å, $b = 60.4$ Å and $c = 133.5$ Å and $\alpha = 90.0°$, $\beta = 90.0°$ and $\gamma = 120.0°$.

The asymmetric unit contains two $BRMS1_{51–98}$ molecules, chains A and B, arranged as a left-

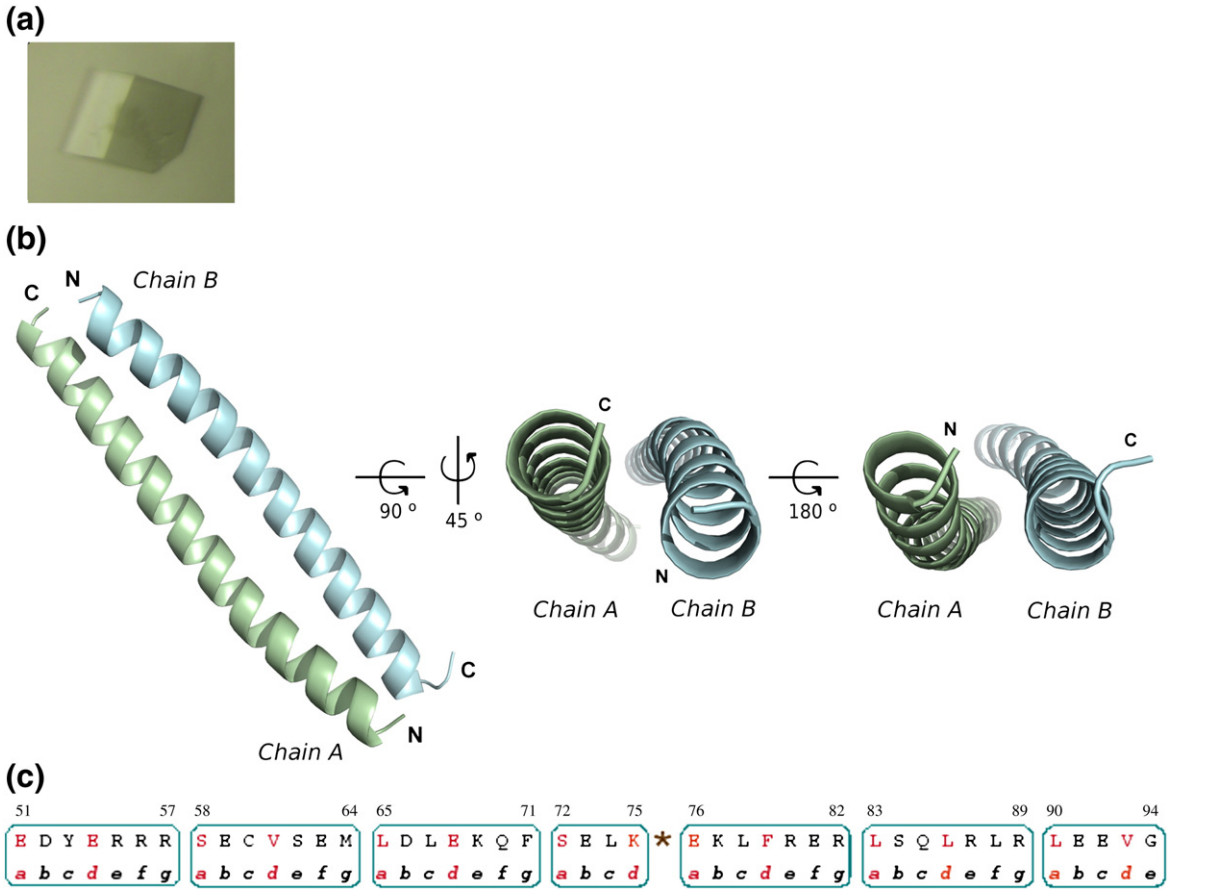

Fig. 1. BRMS1$_{51–98}$ is an antiparallel coiled coil. (a) Crystal of BRMS1 amino-terminal region (residues 51–98) obtained by the hanging-drop vapor-diffusion technique. The crystal was grown using 0.1 M sodium citrate (pH 5.25) and 1.5 M ammonium sulfate in the reservoir. The approximate dimensions of the crystal were 0.25 mm × 0.25 mm × 0.25 mm. (b) Antiparallel coiled coil of amino-terminal BRMS1 region (residues 51–98). The structure was solved by molecular replacement, using the program Phaser[37] (from CCP4) and the 2CCF PDB ID model. The asymmetric unit contains two chains (A and B), which are represented in green (chain A) and in blue (chain B). Amino and carboxylic termini are shown as "N" and "C," respectively. The center and right images, generated upon rotation around *x*- and *y*-axes from the left image, show the twisting of the two antiparallel chains. (c) Heptad repeat assignment of BRMS1$_{51–98}$ established manually. Heptads, with repetition pattern from *a* to *g*, are delimited with boxes. Residues 51–94 of BRMS1 protein are numbered on the top of the assignment and identified with their corresponding letter in the heptad, where the critical positions *a* and *d*, mainly occupied by hydrophobic amino acids, are shown in red. There is a discontinuity or stutter in the heptad pattern localized prior to E76, which is shown with an asterisk.

handed antiparallel coiled coil (Fig. 1b). Residues 95–98 and the initial serine derived from the cloning could not be located in the electron density maps. The final model includes residues E54 to G94 for chain A and E51 to L90 for chain B, 69 water molecules and a sulfate and two chloride ions (Table 1). All residues belong to the preferred regions in the Ramachandran diagram (refinement statistics obtained for the final model are summarized in Table 1). The solved structure contains five complete heptad repeats with a stutter prior to E76 (Fig. 1c), thus following a classical pattern of coiled-coil motifs. The typical heptad repeat is defined in BRMS1$_{51–98}$ by residues E51, S58, L65, S72, E76, L83 and L90 in position *a*, whereas residues E54, V61, E68, K75, F79, L86 and V93 would be occupying position *d* of their respective heptads (Fig. 1c).

The dimeric structure buries a total surface of 1035 Å^2 (calculated by PISA[38]) and is stabilized by hydrophobic interactions, mostly van der Waals contacts, with little polar and electrostatic contribution. Notwithstanding, a salt bridge is established between the N$^{\zeta}$ atom of K75 from chain A and O$^{\epsilon 2}$ of E68 from chain B toward the coiled-coil center (Fig. 2 and Table 2).

The described coiled coil establishes additional interactions with symmetry-related supercoils. In order to establish whether the crystal shows any quaternary structure, we performed an analysis of the possible interfaces, assemblies and surfaces as

Table 1. Data collection and refinement statistics for $BRMS1_{51–98}$ structure

Data collection	
Space group	*H*32
Unit cell dimensions	
a, *b*, *c* (Å)	60.4, 60.4, 133.49
α, β, γ (°)	90, 90, 120
Resolution (last shell) (Å)	48.70–1.91 (2.02–1.91)
Observations (unique)	303,803 (7517)
R_{meas} [a] (%) (last shell)	0.038 (0.287)
Completeness (%) (last shell)	99.7 (100.0)
Multiplicity (last shell)	40.4 (30.9)
Mean $[I/\sigma(I)]$ [b] (last shell)	79.3 (14.5)
Refinement	
Non-hydrogen atoms (solvent molecules)	806 (69)
Heteroatoms	
Cl	2
SO_4	1
R_{work} [c] (R_{free} [d]) (%)	20.3 (27.5)
r.m.s.d. bond length (Å)	0.018
r.m.s.d. bond angles (°)	1.478
B-factor (Å^2)	
Main/side chain	41.7/43.9
Solvent	48.9
Ramachandran (%)	
Favored region	100.0
Outliers	0.0

[a] $R_{meas} = \{\sum_{hkl}[N/(N-1)]^{1/2}\sum_i | I_i(hkl) - \langle I(hkl)\rangle | \}/\sum_{hkl}\sum_i I_i(hkl)$, where $I_i(hkl)$ are the observed intensities, $\langle I(hkl)\rangle$ are the average intensities and N is the multiplicity of reflection *hkl*.

[b] Mean $[I/\sigma(I)]$ is the average of the relation between the intensity of the diffraction and the background.

[c] $R_{work} = \sum_{hkl}\{[F_{obs}(hkl)] - [F_{calc}(hkl)]\}/\sum_{hkl}[F_{obs}(hkl)]$, where $F_{obs}(hkl)$ and $F_{calc}(hkl)$ are the structure factors observed and calculated, respectively.

[d] R_{free} corresponds to R_{work} calculated using 5% of the total reflections selected randomly and excluded during refinement.

implemented in PISA.[38] The antiparallel coiled coil establishes additional interactions with two symmetry-related supercoils via the crystallographic 3-fold axis (Fig. 2). For convenience, chain A symmetry-related molecules have been named A′ and A″. Similarly, chain B symmetry-related molecules have been named B′ and B″.

In the crystal, chain A interacts with chain B″ (Fig. 2a and d) in an antiparallel way, burying a total surface of 583 Å^2. Salt bridges are established between E63 from chain A and R82 from chain B″ and, conversely, between R82 in chain A and E63 in chain B″. An additional salt bridge is established between K75 in chain A and E68 in chain B″ (Fig. 2b and d and Table 2). Chain A also interacts with chain A′ (Fig. 2a), burying a total surface of 276 Å^2. Salt bridges are established between R57 in chain A and E59 or E63 in chain A′ (Fig. 2c and d and Table 2). A third distinct interacting surface is established between chain B and chain B′ (Fig. 2a), burying a total surface of 321 Å^2. This interface also shows the contribution of hydrogen bonds and salt bridges between E59 and E63 from chain B with R56 and R57 from chain B′, respectively (Fig. 2d and Table 2). Finally, electrostatic interactions are also established between K75 from chains A′ and A″ and E68 from chains B and B′, respectively. These residues are located close to the crystallographic ternary axis (Fig. 2b).

In the resulting hexameric arrangement, the N-terminal regions of helices A, A′ and A″ (residues 57–68) establish 3-fold symmetric contacts. In turn, helices B, B′ and B″ are located, at this level, around the periphery of the hexameric ensemble, whereas at the other end of the hexamer, their N-termini similarly form a 3-fold symmetrical arrangement (Fig. 2c and d). Overall, the hexamer buries a total surface area of 14,355 Å^2. Around 42% of the total surface buried by the hexamer corresponds to interactions not directly involved in the formation of the antiparallel coiled coil.

In the hexamer, the thiol groups of C60 from chains A, A′ and A″ are located within disulfide bond distance around the ternary axis. The same arrangement is found in chains B, B′ and B″. Alternative conformers were clearly visible in the electron density maps (see Discussion).

In summary, the X-ray structure reveals a quaternary structure of a trimer of antiparallel coiled coils. This structural arrangement is in agreement with the results obtained from size-exclusion chromatography where the apparent molecular mass of $BRMS1_{51–98}$ was 32 kDa, that is, approximately six times that of the monomer (5.9 kDa). To gather further evidence of this oligomeric state, we performed complementary biophysical studies.

Hydrodynamic measurements

Hydrodynamic measurements of $BRMS1_{51–98}$ were performed in order to determine its translational diffusion coefficient (D) and the corresponding Stoke radius (R) using dynamic light scattering (DLS) and diffusion-ordered spectroscopy nuclear magnetic resonance (DOSY-NMR) (Table 3). Furthermore, analytical ultracentrifugation was also carried out to determine the exact molecular mass of $BRMS1_{51–98}$.

Dynamic light scattering

Using a solution of $BRMS1_{51–98}$ at 1 mg/mL (167 μM), we obtained a maximum of intensity corresponding to a population with 35% of polydispersity, a hydrodynamic radius of 2.6 nm and a molecular mass of 33 kDa (Fig. 3a).

DOSY-NMR experiments

The D value of $BRMS1_{51–98}$ and the corresponding Stokes radius R are shown in Table 3; the values correspond to the average of three measurements. The theoretical ideal value of the hydrodynamic

radius for an unsolvated spherical molecule, R_t, is given by $R_t = \sqrt[3]{3M\bar{V}/4N_{Av}\pi}$, where $\bar{V}$ is the specific volume (0.70 cm^3/g, which is the mean of the 20 amino acids), N_{Av} is Avogadro's number and M is the molecular mass (5.9 kDa for monomeric $BRMS1_{51–98}$). That expression yields an R of 1.18 nm for $BRMS1_{51–98}$. This value is very different to that measured experimentally, suggesting that either the sample could correspond to a self-associating protein or, alternatively, the protein could be largely disordered.

Using an empirical function, we can estimate the expected R for monomeric $BRMS1_{51–98}$ to be between 1.47 nm, assuming that it is a folded protein [$R = (4.75 \pm 1.11)N^{0.29 \pm 0.02}$, where N is the number of residues[39]], and 2.09 nm, if $BRMS1_{51–98}$ behaves as a random coil with disordered species [$R = (0.027 \pm 0.01)M^{0.50 \pm 0.01}$, where M is the molecular mass[40]]. The experimental R of the $BRMS1_{51–98}$ species is larger than these theoretical boundaries, and therefore, it does not adjust to a monomeric folded protein or to a monomeric unfolded protein.

As mentioned previously, C60 from different chains fall in close vicinity within the hexameric quaternary structure. Although the structure does not suggest the formation of disulfide bridges, the DOSY-NMR analysis was also performed in the presence of 1 mM DTT (data not shown), obtaining similar results and therefore suggesting that disulfide bridges do not play a role in $BRMS1_{51–98}$ oligomerization state.

Analytical ultracentrifugation: Heterogeneity and sedimentation coefficient distributions of $BRMS1_{51–98}$

Size-exclusion chromatography had shown that $BRMS1_{51–98}$ elutes as a 32-kDa protein on a Superdex 75 26/60 or Superdex 75 PC3.2/30 gel-filtration column using 20 mM Tris–HCl (pH 7.5) and 50 mM NaCl buffer. Identical results were obtained along protein concentrations from 83.5 to 9 μM and also in the presence of 2 mM DTT (data not shown). The estimated molecular mass is in agreement with the hexameric quaternary structure found in the crystallographic structure of $BRMS1_{51–98}$. However, given that size-exclusion molecular mass estimations are not independent of molecular shapes, we decided to perform analytical ultracentrifugation analysis in order to further confirm the oligomeric state of $BRMS1_{51–98}$.

Sedimentation velocity experiments were carried out at 1, 0.5, 0.2, 0.1 and 0.05 mg/mL, which correspond to 167, 83.5, 33.4, 16.7 and 8.35 μM, respectively, to measure the rate at which $BRMS1_{51–98}$ molecules migrate in response to a centrifugal force. The $c(s)$ profile of the protein obtained in the velocity experiment analysis (Fig. 3b) shows two peaks at 1 mg/mL: a predominant component, at 93.1%, with a sedimentation coefficient of 2.7 ± 0.1 S and a minor component (5.5%) of 1.5 ± 0.1 S. The minor component was undetectable at lower concentrations, and the unique peak presented a sedimentation coefficient of 2.8 ± 0.1 S (Fig. 3b).

Sedimentation equilibrium experiments (Fig. 3c) were also carried out in parallel to determine the molecular mass of $BRMS1_{51–98}$. Experimental data fitted with a model of single species and resulted in molecular masses of around 34 kDa at a concentration of 167 μM and 36 kDa in the 83.5- to 8. 35-μM concentration range. The high quality of the fitting to the model is shown in Fig. 3c.

Discussion

$BRMS1_{51–98}$ is an antiparallel coiled-coil motif

Despite its biological importance, structure–function studies on BRMS1 have remained elusive until now. Here, we show that the $BRMS1_{51–98}$ fragment has structural integrity when isolated from the rest of the protein. The structure of the $BRMS1_{51–98}$ fragment shows a left-handed antiparallel coiled coil, with heptad repeat positions *a* and *d*, which form the "knob-into-holes" packing typical of coiled coils, filled by seven polar residues and seven hydrophobic residues. Positions *a* and *d* are occupied by hydrophobic residues at the C-terminus of the molecule, whereas positions *e* and *g* are mainly taken up by polar residues, Arg being the most representative amino acid. These two characteristics, in addition to the stutter discontinuity that appears prior to E76 in $BRMS1_{51–98}$, are the most commonly observed consensus features described in coiled-coil motifs.[34,35] The observed coiled coil extends at least between residues 51 and 94, which are clearly seen in the electron density maps and could be assigned to canonical heptad repeats (Fig. 1c). This observation further extends the lengthiest coiled-coil assignment based solely on the sequence, which defined the carboxylic end of the N-terminal coiled coil at residue 81 (Ncoils 1.0,[29] predicts a coiled coil between residues 49 and 81 with a probability higher than 0.8) (Fig. 3d).

$BRMS1_{51–98}$ is a self-associating protein with potential to mediate oligomerization

Analysis of the interacting surfaces in the crystal structure shows that $BRMS1_{51–98}$ can self-associate in the absence of the rest of the protein, oligomerize as a homo-hexamer consisting of a trimer of antiparallel coiled coils (Fig. 2a). The oligomerization state of $BRMS1_{51–98}$ is not sustained by any disulfide bonds, since DOSY-NMR experiments gave identical hydrodynamic results in the presence

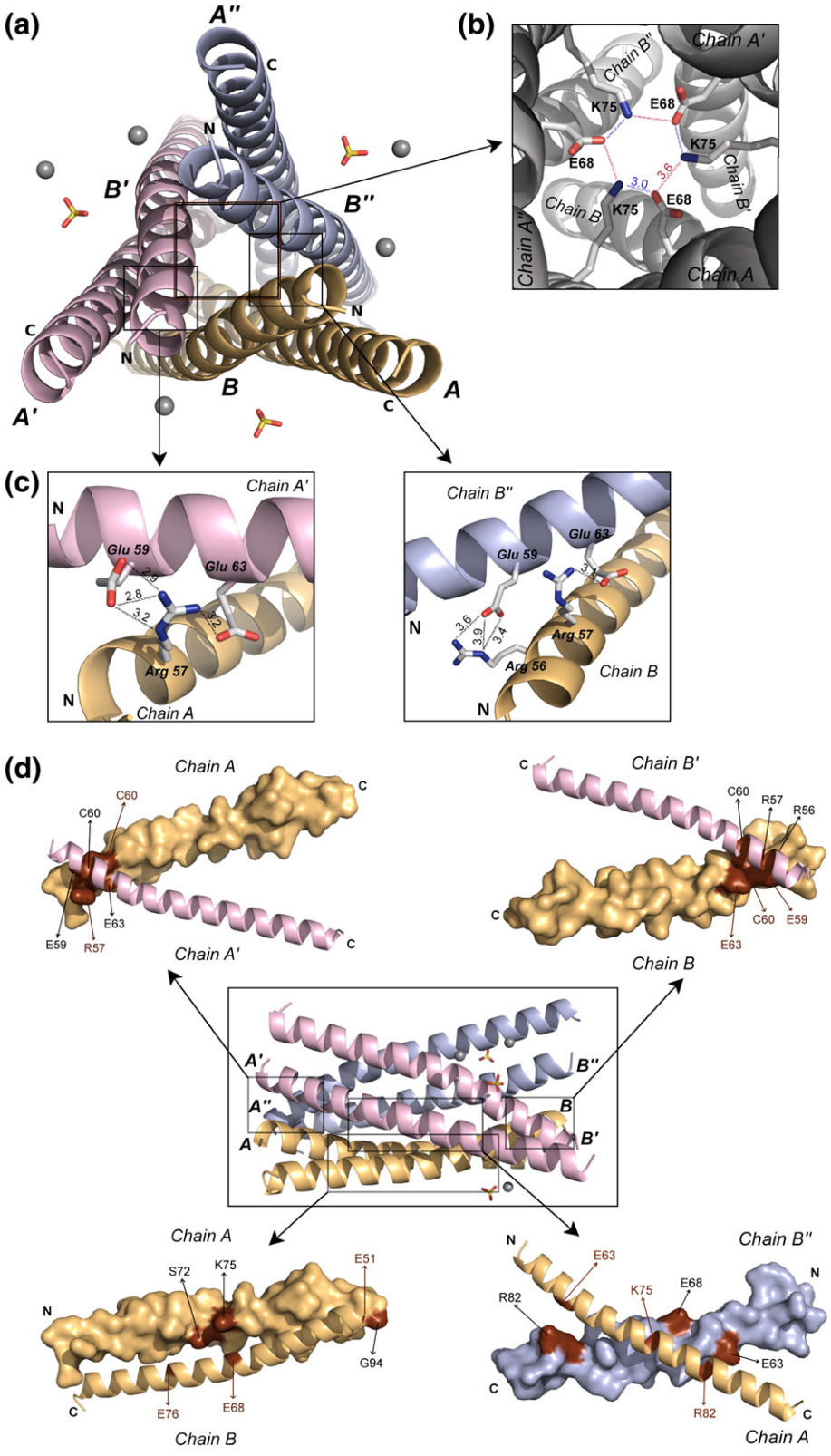

Fig. 2 (*legend on next page*)

Table 2. Contacts and interfaces within the hexamer

	Interface (Å^2)	Hydrogen bonds		Distance (Å)	Salt bridges		Distance (Å)
A–B (A′–B′/A″–B″)	1034.8	A: Gly94 [O]	B: Glu51 [N]	3.29	A: Lys75 [N$^{\zeta}$]	B: Glu68 [O$^{\varepsilon 2}$]	3.07
		A: Ser72 [O$^{\gamma}$]	B: Glu76 [O$^{\varepsilon 2}$]	3.06			
A–B″ (A′–B/A″–B′)	582.7				A′: Glu63 [O$^{\varepsilon 1}$]	B: Arg82 [N$^{\varepsilon}$]	3.94
					[O$^{\varepsilon 2}$]	[N$^{\varepsilon}$]	2.60
					[O$^{\varepsilon 1}$]	[NH1]	3.32
					[O$^{\varepsilon 2}$]	[NH1]	3.16
					A′: Arg82 [NH1]	B: Glu63 [O$^{\varepsilon 1}$]	2.81
					[N$^{\varepsilon}$]	[O$^{\varepsilon 1}$]	3.51
					[NH1]	[O$^{\varepsilon 2}$]	3.38
					[N$^{\varepsilon}$]	[O$^{\varepsilon 2}$]	2.59
					A′: Lys75 [N$^{\zeta}$]	B: Glu68 [O$^{\varepsilon 2}$]	3.56
A–A′ (A′–A″/A″–A)	276.1	A: Cys60 [S$^{\gamma}$]	A′: Cys60 [O]	3.72	A: Arg57 [N$^{\varepsilon}$]	A′: Glu59 [O$^{\varepsilon 2}$]	3.23
					[NH2]	[O$^{\varepsilon 1}$]	2.87
					[NH2]	[O$^{\varepsilon 2}$]	2.78
					A: Arg57 [NH1]	A′: Glu63 [O$^{\varepsilon 1}$]	3.25
B–B′ (B′–B″/B″–B)	321.4	B: Glu59 [O]	B′: Arg57 [NH1]	3.73	B: Glu59 [O$^{\varepsilon 1}$]	B′: Arg56 [N$^{\varepsilon}$]	3.45
					[O$^{\varepsilon 2}$]	[N$^{\varepsilon}$]	3.97
					[O$^{\varepsilon 2}$]	[NH1]	3.60
		B: Cys60 [O]	B′: Cys60 [S$^{\gamma}$]	3.75	B: Glu63 [O$^{\varepsilon 1}$]	B′: Arg57 [NH1]	3.12

Interfaces, hydrogen bonds and salt bridges established between chains A and B of the asymmetric unit and symmetry-related chains (′ and ″). The contacting atom from each residue is shown with brackets. These analyses were carried out with Contact (from CCP4 suite[46]) and PISA[38] softwares.

or in the absence of 1 mM DTT. Moreover, identical results were obtained in size-exclusion chromatography in the absence or presence of 2 mM DTT, indicating that no disulfide bridges are involved in oligomerization. The alternate conformations of C60 side chains observed in the crystal are compatible with a static disorder resulting from different combinations of two C60 residues engaged in a disulfide bond and one free C60 residue. Consistent with the results obtained in solution, the dihedral angle around these bonds is only ~20°, implying that they are very weak and easily reduced disulfide bonds.

The Stoke radii obtained from DLS and DOSY-NMR (2.6 nm and 2.52 nm, respectively) agree remarkably well with the 2.7 nm calculated by HYDROPRO[41] from the structure of the hexameric form of the BRMS1$_{51–98}$ fragment. In fact, we also used HYDROPRO to estimate the value of *D* from the hexameric structure, which produced a value of 7.99×10^{-7} cm^2 s^{-1}, very close to the experimentally determined 7.3×10^{-7} cm^2 s^{-1} and strongly supporting the idea that the hexamer observed in the crystal also exists in solution.

Analytical ultracentrifugation experiments allow the measurement of the molecular mass of a particle independently of its shape and also the performance of protein association studies.[42] Both DLS and sedimentation velocity analytical ultracentrifugation showed that, at a concentration of 167 μM,

Fig. 2. The BRMS1$_{51–98}$ hexamer. (a) Cartoon representation of BRMS1$_{51–98}$ quaternary structure formed by a trimer of antiparallel coiled coils packed around a ternary axis. This hexamer is built by the interaction of the two chains of the asymmetric unit with four of their symmetry-related molecules. Chains are labeled as A (chain A) and B (chain B). Labels A′ and A″ and B′ and B″ refer to symmetry-related chains A and B, respectively. The two molecules of each coiled coil are represented with the same color: light brown for A–B, pink for A′–B′ and blue for A″–B″. Carboxylic and amino terminals are shown as C and N, respectively. Chloride and sulfate ions are represented as spheres and sticks, respectively. (b) Detail of salt bridges established between K75 from chain A and symmetry-related chains A (A′ and A″) and E68 from chain B and symmetry-related chains B (B′ and B″), around the ternary axis. Distances between O$^{\varepsilon 2}$ atom of E68 and N$^{\zeta}$ atom of K75 are represented as color-coded lines as follows: 3. 56-Å distance in red and 3.07 Å in blue. (c) Detail of the N-terminal salt bridges within symmetry-related chain groups A–A′–A″ (on the left) and B–B′–B″ (on the right). N abbreviation represents the amino termini. The hydrogen bonds (with distances shown in angstroms) between nitrogen and oxygen atoms of arginines and glutamic acids, respectively, are represented with dotted lines. (d) Interacting surfaces among the different chains (A and B, in light brown) and symmetry-related molecules (pink and blue) established within the hexameric conformation. Each panel contains a distinct contact surface, concretely from pairs A–A′, B–B′, A–B and A–B″ (which are also detailed in Table 2). One molecule is represented as a ribbon cartoon, and the other one, as a molecular surface. The interacting residues are marked in dark brown in both chains. N and C letters indicate the amino and carboxylic ends of the molecule. A different orientation of the hexamer, resulting from a 90° rotation in the *y*-axis with respect to (a), is shown in the center.

Table 3. Hydrodynamic measurements of $BRMS1_{51–98}$ species

D ($cm^2\ s^{-1}$)	R (nm)	R^a (nm)	R^b (nm)
$(7.3 \pm 0.2) \times 10^{-7}$	2.52	1.47 ± 0.1	2.09 ± 0.01

[a] Calculated by the mathematical expression of Wilkins *et al.* assuming that the $BRMS1_{51–98}$ species is a monomeric folded protein.[39]

[b] Calculated by the mathematical expression of Danielsson *et al.* assuming that the $BRMS1_{51–98}$ species is a monomeric unfolded protein.[40]

$BRMS1_{51–98}$ is found in solution as two molecular species. Given that the molecular mass of monomeric human $BRMS1_{51–98}$ is 5.9 kDa and taking into account the frictional ratio calculated by the SedFit software (~1.4), human $BRMS1_{51–98}$ behaves predominantly as a hexamer of around 39 kDa, accounting for 93.1% of the total mass, while a remaining 5.5% of the mass shows a dimeric behavior (16 kDa). Subsequent experiments at 0.5, 0.2, 0.1 and 0.05 mg/mL only showed the hexameric signal (Fig. 3b), with an apparent molecular mass of 36 kDa. Moreover, $BRMS1_{51–98}$ sedimentation equilibrium experimental data resulted in average molecular masses of around 34 kDa and 36 kDa for 167 μM and the 83.5 to 8.35–μM range, respectively, in line with those determined by size-exclusion chromatography in an outgoing sample column concentration range of 83.5–9 μM (32 kDa) and DLS at 167 μM (33 kDa). Finally, theoretical analysis of the interaction surfaces involved in the formation of

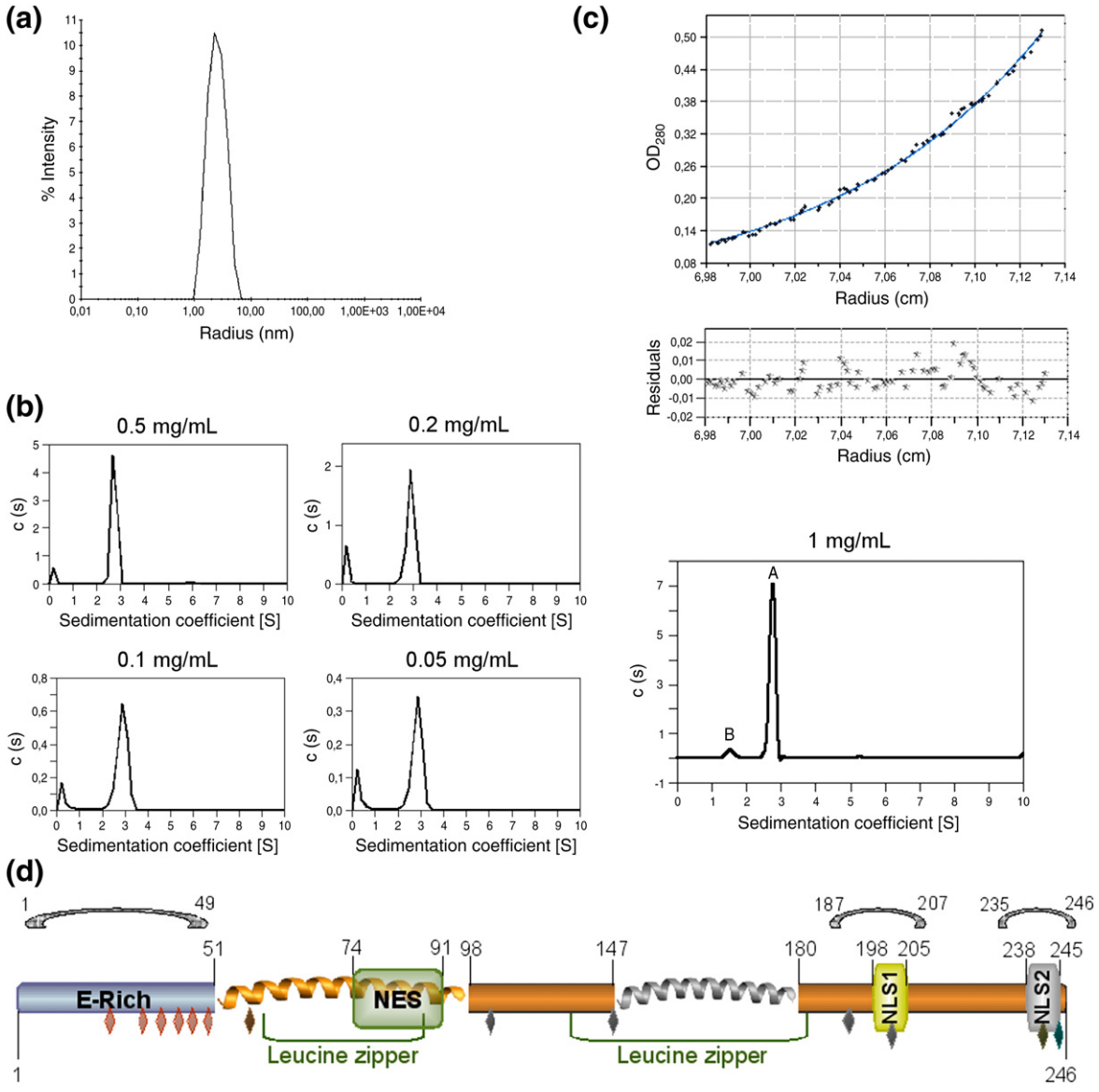

Fig. 3 (*legend on next page*)

the hexamer, performed with the PISA software,[38] suggests that this oligomer is the most stable quaternary structure in solution. Altogether, these results strongly support the notion that, at a protein concentration as low as 0.05 mg/mL (8.35 μM), $BRMS1_{51–98}$ already forms in solution the hexameric arrangement that we find in its crystal structure.

The closest structural similarity of $BRMS1_{51–98}$ is with the membrane-proximal ectodomain region of the envelope glycoprotein gp41 subunit from human immunodeficiency virus type 1 [Protein Data Bank (PDB) ID 3G9R], a transmembrane glycoprotein involved in the membrane-fusion process of cellular and viral membranes that takes place during human immunodeficiency virus type 1 infection. Despite a sequence identity of only 5%, the α-carbon r.m.s.d. between $BRMS1_{51–98}$ and gp41 is 0.5 Å for 40 residues. The best overlap is with gp41 membrane-proximal ectodomain region in a putative prefusion conformation;[43] however, the postfusion state of gp41 including the inner core and outer layer of the gp41 ectodomain resembles that of $BRMS1_{51–98}$, since it is formed by a trimer of α-helical hairpins that plays a critical role in the membrane fusion of the virus.[44] There is, however, no conservation between the relative orientations of the helices in the two structures.

Implications for BRMS1 cellular localization

At this stage, it is worth mentioning that the molecular mass of monomeric full-length BRMS1 would allow passive diffusion of the protein through the channel of the nuclear pore complex. However, BRMS1 contains a functional NLS that interacts with importin α6. Furthermore, BRMS1 is also actively exported from the nucleus to the cytoplasm.[33] Indeed, we have previously identified a NES involving BRMS1 residues 74–91 that partially overlaps with the C-terminal part of the coiled-coil fragment $BRMS1_{51–98}$[33] (Fig. 3d). Three out of the four consensus hydrophobic residues for the NES are not accessible in the coiled coil and occupy position *a* (L83) or *d* (F79 and L86) of the heptad repeat. This suggests that the coiled coil would require monomerization of the individual helices prior to its interaction with the nuclear exportins. Taken together, our findings suggest that BRMS1 might be part of a larger molecular entity with highly dynamic properties. Further experiments will be necessary to ascertain *in vivo* the existence and the composition of BRMS1 oligomers, which could, in principle, involve a BRMS1 hexamer built on the $BRMS1_{51–98}$ assembly that we have described.

$BRMS1_{51–98}$ may establish molecular clusters

Coiled-coil regions are well-known protein–protein interaction modules.[34,35] Our results confirm that $BRMS1_{51–98}$ is indeed a coiled-coil region that could allow BRMS1 to establish homo- or hetero-oligomerization contacts. Actually, a number of proteins do interact with BRMS1 through their coiled-coil motifs, for example, AT-rich interactive domain 4A, which participates in the DNA remodeling complex Sin3–HDAC,[18] or the SNX6 protein.[21] In fact, residues 300–406 from SNX6 have been shown to interact with residues 1–88 from BRMS1.[21] Since this SNX6 region includes a putative coiled coil, we anticipate that this is a coiled-coil-mediated interaction. This interaction is

Fig. 3. Hydrodynamic measurements in $BRMS1_{51–98}$ and schematic representation of structure motifs of the BRMS1 full-length protein. (a) DLS of $BRMS1_{51–98}$ at a protein concentration of 167 μM in a buffer containing 20 mM Tris–HCl (pH 7.5) and 50 mM NaCl at 293 K. The highest peak of intensity corresponds to a hydrodynamic radius of 2.6 nm with a polydispersity of 35% and an apparent molecular mass of 33 kDa. (b) Sedimentation velocity data for $BRMS1_{51–98}$ at 167 μM (1 mg/mL), 83.5 μM (0.5 mg/mL), 33.4 μM (0.2 mg/mL), 16.7 μM (0.1 mg/mL) and 8.35 μM (0.05 mg/mL), monitored using Rayleigh interferometric detection (1 mg/mL sample) and by absorbance at a wavelength of 230 nm (the rest of samples). The experiment was carried out at 293 K and 48,000 rpm and in 20 mM Tris–HCl (pH 7.5) and 50 mM NaCl. Differential coefficient distribution [$c(s)$] was fitted using the SedFit software.[22] The $c(s)$ curve suggests that $BRMS1_{51–98}$ at 1 mg/mL presents a predominant species (peak A) at 93.1% with a sedimentation coefficient of 2.7 ± 0.1 S and a second peak (B, 5.5%) with 1.5 ± 0.1 S, and the range from 0.5 mg/mL to 0.05 mg/mL protein sample shows a unique peak of 2.8 ± 0.1 S. The apparent molecular masses (16 kDa and 39 kDa for peaks B and A, respectively, at 1 mg/mL and 36 kDa for the unique peak at 0.5–0.05 mg/mL range) were calculated from the $c(s)$ distribution, with a frictional ratio of 1.4. (c) Equilibrium sedimentation assay for the $BRMS1_{51–98}$ sample at 167 μM was conducted at 293 K and with scan data acquisition at 280 nm and at 14.5, 19 and 28 krpm of velocity. The residuals (lower panel) show the fitting between the experimental data and an ideal single-species model (blue line). (d) The amino acid boundaries identified by different prediction servers such as Disopred,[23] Porter,[24] DisEMBL[25] or Poodle[26] for unfolded regions; Paracoil,[27] Multicoil[28] or Coils[29] for coiled-coil motifs; or Scansite,[30] PSORT II[31] or HPRD[32] for phosphorylation sites, retention and NLSs[4] are shown with numbers. Blue, green, yellow and gray boxes show the glutamic-rich region (E-rich), functional NES,[33] functional NLS (NLS1)[33] and predicted NLS (NLS2), respectively. Two predicted imperfect leucine zipper motifs are shown with brackets. The rhombi represent putative phosphorylation sites: red for casein kinase II, brown for cAMP/cGMP and gray for protein kinase C. The green rhombus at the C-terminal corresponds to an endoplasmic reticulum retention signal. The experimentally determined first coiled-coil motif (from 51 to 98 residues) and the second predicted coiled coil are represented as orange and gray helices, respectively. The predicted unfolded regions with their corresponding boundaries are shown as an archway over the scheme.

of particular relevance since SNX6 is part of the retromer complex, involved in the transport of transmembrane cargo proteins from endosomes to the trans-Golgi network. Furthermore, SNX6 interacts with transforming growth factor β receptors, which have largely been involved in metastasis.

The crystallographic quaternary structure of the $BRMS1_{51–98}$ fragment provides clues about the interaction of BRMS1 with other cellular partners through its N-terminal coiled coil, which we have proved to be longer than what was predicted from its sequence. Thus, this particular molecular arrangement might suggest the ability of BRMS1 to promote molecular clustering through its N-terminal coiled-coil region.

A second region in the BRMS1 sequence is predicted to form a coiled coil around residues 147–180 that varies in length depending on the predictions tools used. In light of our observations, the real coiled coil might extend further, especially if we take into account that the predictions are less favorable for this C-terminal coiled coil. Recent reports have shown that both coiled-coil regions of BRMS1 are involved in hetero-association with other proteins. However, we have also shown that at least the N-terminal coiled coil is also capable of establishing homo-oligomers. Additional studies should establish whether the second coiled coil is able to undergo a similar homo-oligomerization mechanism.

Conclusion

The X-ray crystal structure that we report represents the first structural work on the human BRMS1 protein or any of its orthologs, opening new avenues to explore the function of this otherwise elusive protein. Together with the hydrodynamic data that we have gathered from a wide range of techniques, this structure shows that the predicted N-terminal coiled-coil region of BRMS1 protein does actually form an antiparallel coiled-coil motif with a capability of mediating oligomerization. Our observations suggest that BRMS1 biological function could be marked by an ability to establish molecular clusters. Alternatively, the N-terminal coiled coil of BRMS1 protein could be involved in more restricted oligomerization in order to perform other biological functions, such as the modulation of transcription. Further efforts will test the validity of these hypotheses.

Materials and Methods

Protein expression and purification

The DNA fragment encoding the first predicted coiled-coil motif of human BRMS1 including amino acids 51–98 ($BRMS1_{51–98}$) was amplified from RZPD cDNA clone ID: IRALp962L0425Q2 by PCR using forward $^{5'}$GCG-ggatcc-GAGGACTATGAGCGACGCC$^{3'}$ and reverse $^{5'}$CGC-ctcgag-TTAGGCTCTCTCAGCCCC$^{3'}$ primers that contain restriction sites shown in lowercase to facilitate the cloning. The amplicon was subcloned into a modified version of plasmid pET28 (Novagen) that allows the expression of an N-terminally 6×His-SMT3 fusion protein.[45] After cleavage with a SMT3-specific protease ULP, a serine residue is introduced at the N-terminus. The DNA-sequence-verified construct was transformed into Rosetta(DE3)pLysS *E. coli* cells for His-SMT3-$BRMS1_{51–98}$ fusion protein expression.

Overproduction of the target protein was carried out at 310 K using 2xTY medium (twice-concentrated tryptone–yeast extract; 16 g/L tryptone, 10 g/L yeast extract and 85 mM NaCl, pH 7.2). The expression was induced by addition of 1 mM IPTG when the optical density at 600 nm reached a value of 0.7, and cells were harvested after 4 h and resuspended in lysis buffer [50 mM Tris–HCl (pH 7.5), 500 mM NaCl, 0.5% Tween 20 and 0.2 mM 4-(2-aminoethyl) benzenesulfonyl fluoride hydrochloride (Sigma)].

After cell lysis by sonication and removal of cell debris by centrifugation (30 min at 20,000*g*), the fusion protein was histidine affinity purified using 5-mL Hi-Trap Chelating columns (GE Healthcare) previously loaded with nickel sulfate, washed with 50 mM Tris–HCl (pH 7.5), 150 mM NaCl and 10 mM imidazole and eluted with a linear gradient against 50 mM Tris–HCl (pH 7.5), 150 mM NaCl and 500 mM imidazole. The SMT3-specific protease ULP was added to the eluate in a 1:1000 concentration (protease weight:protein weight), and the mixture was dialyzed overnight at 277 K, against 50 mM Tris–HCl (pH 7.5) and 150 mM NaCl, using "Slide-A-Lyzer Dialysis Cassettes" of 3.5-kDa cutoff (Pierce). For removal of His-SMT3, the sample underwent a second histidine-affinity purification step. The flow-through fraction was loaded in a size-exclusion Superdex 75 26/60 column (GE Healthcare) equilibrated with 20 mM Tris–HCl (pH 7.5) and 50 mM NaCl at 277 K. Fractions containing highly purified protein, as estimated by SDS-PAGE electrophoresis and Coomassie staining, were further concentrated with ultrafiltration devices (5-kDa cutoff; Millipore), flash cooled under liquid nitrogen and stored at 193 K until use.

Structure determination

Protein crystallization and X-ray data collection

Initial crystallization trials were performed on a Cartesian Honeybee robot (Digilab) using commercial kits and various protein concentrations. After evaluation of initial hits, optimized crystals were obtained by the hanging-drop vapor-diffusion method at 295 K. Briefly, 1 μL of purified $BRMS1_{51–98}$ protein at 50 mg/mL was mixed with 1 μL of reservoir solution [0.1 M sodium citrate (pH 5.25) and 1.5 M ammonium sulfate] and equilibrated against 0.5 mL of reservoir solution. Crystals were cryoprotected using paratone-N (Hampton Research), mounted on cryo-loops and flashed cooled at 100 K under a cryogenic nitrogen stream. The diffraction data (Table 1) were collected on the ID14eh4 beamline at the European Synchrotron Radiation Facility (Grenoble,

France) at a wavelength of 1.2785 Å and using a Q315r ADSC X-ray detector. The images were collected using the beamline software MXCuBE (*MX Cu*stomised *B*eamline *E*nvironment).

Data reduction was performed using MOSFLM for reflection, indexing and integration and SCALA for scaling and merging, both from the CCP4 program suite.[46]

Structure determination and refinement

The three-dimensional structure of $BRMS1_{51–98}$ was solved by automated search with Phaser[37] using coordinates from PDB ID 2CCF as a molecular replacement model. This model refers to residues 249–281 of the yeast transcriptional activator GCN4 and includes two chains with 31 residues modeled in chain A and 32 residues in chain B.[47] The search of a good rotation and translation solution was carried out by defining two individual ensembles, one containing the chain A and the second one with the chain B, and looking for one copy from each. The resulting model was modified and completed manually in the real space by Coot,[48] with alternating refinement cycles in the reciprocal space using Refmac5[49] with TLS[50] and Babinet scaling. The TLS groups were selected using the internet web tool TLSMD.[51]

Real-space correlation, coordinate errors, R, R_{free}, *B*-factors and r.m.s.d. were checked using Sfcheck, PROCHECK[52] and Baverage (CCP4[46]). MolProbity[53] and Monster[54] and Contact (from CCP4[46]) were used for the geometric and contact analyses, and AreaIMol (CCP4 package[46]) and PISA software[38] were used to explore macromolecular interfaces and assemblies.

Dynamic light scattering

DLS measurements in obtaining hydrodynamic radii of $BRMS1_{51–98}$ protein were carried out at 293 K with a DynaPro™ instrument (Protein Solutions), using a quartz cuvette of 3-mm path length. Protein samples (1 mg/mL) in 20 mM Tris–HCl (pH 7.5) and 50 mM NaCl were centrifuged for 10 min at 16,000*g* prior to measurements. Thirty readings were collected with a 5-s acquisition time and 100% of incident beam power. The data were visualized and analyzed using the Dynamics V6 software to obtain the hydrodynamic radius of the particles and the apparent molecular size and the homogeneity of the sample.

DOSY-NMR experiments

The NMR experiments were acquired on an Avance DRX-500 spectrometer (Bruker GmbH, Karlsruhe, Germany) equipped with a triple-resonance probe and z-pulse field gradients.

NMR samples for DOSY-NMR spectra were prepared by concentrating the samples in Centriprep devices (5-kDa cutoff; Millipore) in a H_2O:D_2O (1:9) solution. The solution was centrifuged briefly to remove insoluble protein and then transferred to a 5-mm NMR tube at 293 K. The final protein concentrations of $BRMS1_{51–98}$ were in the range 100–150 μM. The pH of the sample was 6.9 (50 mM sodium phosphate buffer). The values of the pH reported here represent the apparent values of pH, without correction for isotope effects. 3-Trimethylsilylpropionic-2,2,3,3-d_4 was used as the internal chemical shift reference.

Translational self-diffusion measurements were performed with the pulsed-gradient spin-echo sequence. The following relationship exists between the translational self-diffusion parameter D and the delays during acquisition:[55]

$$\frac{I}{I_0} = -\exp\left(D\gamma_H^2\delta^2G^2\left(\Delta - \frac{\delta}{3} - \frac{\tau}{2}\right)\right)$$

where I is the measured peak intensity of a particular (or a group of) resonance(s), I_0 is the maximum peak intensity of the same resonance(s) at the smaller gradient strength, D is the translational self-diffusion constant (in square centimeters per second), δ is the duration (in seconds) of the gradient, G is the gradient strength (in Tesla per centimeter), Δ is the time (in seconds) between the gradients, γ_H is the gyromagnetic constant of the proton and τ is the recovery delay between the bipolar gradients (100 μs). Data are plotted as I/I_0 *versus* G^2, and the exponential factor of the resulting curve is $D\gamma_H^2\delta^2\left(\Delta - \frac{\delta}{3} - \frac{\tau}{2}\right)$, from where D can be easily obtained. The duration of the gradient was varied between 2.6 and 3 ms, and the time between both gradients was 150 ms. The most upfield-shifted methyl groups (those between 0.5 and 1 ppm) were used to measure the intensity changes.

The value of the Stokes radius R was determined as described by Wilkins *et al.*[39] Briefly, 0.1% of dioxane was added to the $BRMS1_{51–98}$ sample, and its D was calculated. Since the R of dioxane is 2.12 Å, the R of the protein can be obtained.

Analytical ultracentrifugation

The sample protein at 1, 0.5, 0.2, 0.1 and 0.05 mg/mL (corresponding to 167, 83.5, 33.4, 16.7 and 8.35 μM, respectively) in buffer containing 20 mM Tris–HCl (pH 7.5) and 50 mM NaCl was precleared at 16,000*g* before ultracentrifugation protocol. The analytical ultracentrifugation experiments were conducted at 293 K.

Velocity measurements

Sedimentation velocity experiment was performed on an Optima XL-I (Beckman, CA), using an AnTi50 rotor and a standard double-sector Epon-charcoal center pieces (1. 2-cm optical path length). Four hundred microliters of sample and reference solution was loaded and sedimented at 48,000 rpm for 3 h and 30 min, registering successive entries every minute. The evolution of the resulting concentration gradient of material in the cell as a function of time and radial position was monitored using Rayleigh interferometric detection in the case of the sample at 1 mg/mL and by absorbance at a wavelength of 230 nm in the rest of the samples (0.5–0.05 mg/mL range).

Differential sedimentation coefficient distributions [$c(s)$] were calculated by least-squares boundary modeling of sedimentation velocity data using the SedFit software (Version 11.8) as described previously.[22] The calculated frictional ratios were used to transform the $c(s)$ distribution into the corresponding molar mass distribution.[56,57]

Sedimentation equilibrium

An Optima XL-A (Beckman) analytical ultracentrifuge equipped with UV–visible absorbance optics was employed for analytical ultracentrifugation measurements by using an An50Ti rotor. Short-column (85 μL) sedimentation equilibrium runs were carried out at multiple speeds (14.5, 19, and 28 krpm in the 1 mg/mL sample and 16, 19 and 22 krpm in the 0.5–0.05 mg/mL range) by taking absorbance scans at wavelengths 280 nm (for 1 mg/mL) and 240–230 nm (for 0.5–0.05 mg/mL range). After the equilibrium scans, a high-speed centrifugation run at 45 krpm was performed to estimate the corresponding baseline offsets.

The weight-average buoyant molecular mass of $BRMS1_{51–98}$ was calculated using the Hetero-Analysis program (Version 1.1.33).[58] The molecular mass of the protein was determined from the experimental buoyant masses using the values of 0.7255 cm^3/g and 1.00087 g/cm^3 as the partial specific volume and density, respectively.

PDB accession numbers

Coordinates and structure factors have been deposited in the PDB with accession number 2XUS.

Acknowledgements

This work was supported by Ministerio de Ciencia e Innovación (SAF2008-04048-E and SAF2009-10667); Conselleria de Sanitat, Generalitat Valenciana (AP-001/10); Consejo Superior de Investigaciones Científicas (200820I020); and Fundación Mutua Madrileña, Spain. Work in JLN laboratory was supported by Ministerio de Ciencia e Innovacion (CSD2008-00005, SAF2008-05742-C2-01), Generalitat Valenciana (ACOMP2011/113) and Fundación para la investigación y prevención del SIDA en España, FIPSE, (36557/06).

The authors thank Carlos Alfonso (Servicio de Ultracentrifugación Analítica, Centro de Investigaciones Biológicas, CSIC) for analytical ultracentrifugation and the European Synchrotron Radiation Facility staff at ID14-4 for technical support and assistance during X-ray data collection.

The authors acknowledge C. D. Lima for kindly supplying the modified version of pET28 over-expressing SMT3 tag.

References

1. Rinker-Schaeffer, C. W., O'Keefe, J. P., Welch, D. R. & Theodorescu, D. (2006). Metastasis suppressor proteins: discovery, molecular mechanisms, and clinical application. *Clin. Cancer Res.* **12**, 3882–3889.
2. Steeg, P. S. (2003). Metastasis suppressors alter the signal transduction of cancer cells. *Nat. Rev., Cancer*, **3**, 55–63.
3. Steeg, P. S., Ouatas, T., Halverson, D., Palmieri, D. & Salerno, M. (2003). Metastasis suppressor genes: basic biology and potential clinical use. *Clin. Breast Cancer*, **4**, 51–62.
4. Seraj, M. J., Samant, R. S., Verderame, M. F. & Welch, D. R. (2000). Functional evidence for a novel human breast carcinoma metastasis suppressor, BRMS1, encoded at chromosome 11q13. *Cancer Res.* **60**, 2764–2769.
5. Shevde, L. A., Samant, R. S., Goldberg, S. F., Sikaneta, T., Alessandrini, A., Donahue, H. J. *et al.* (2002). Suppression of human melanoma metastasis by the metastasis suppressor gene, *BRMS1*. *Exp. Cell Res.* **273**, 229–239.
6. Li, J. & Li, G. (2010). Cell cycle regulator ing4 is a suppressor of melanoma angiogenesis that is regulated by the metastasis suppressor BRMS1. *Cancer Res.* **70**, 10445–10453.
7. Zhang, S., Lin, Q. & Di, W. (2006). Suppression of human ovarian carcinoma metastasis by the metastasis-suppressor gene, *BRMS1*. *Int. J. Gynecol. Cancer*, **16**, 522–531.
8. Metge, B. J., Frost, A. R., King, J. A., Dyess, D. L., Welch, D. R., Samant, R. S. & Shevde, L. A. (2008). Epigenetic silencing contributes to the loss of BRMS1 expression in breast cancer. *Clin. Exp. Metastasis*, **25**, 753–763.
9. Nagji, A. S., Liu, Y., Stelow, E. B., Stukenborg, G. J. & Jones, D. R. (2010). BRMS1 transcriptional repression correlates with CpG island methylation and advanced pathological stage in non-small cell lung cancer. *J. Pathol.* **221**, 229–237.
10. Saunders, M. M., Seraj, M. J., Li, Z., Zhou, Z., Winter, C. R., Welch, D. R. & Donahue, H. J. (2001). Breast cancer metastatic potential correlates with a breakdown in homospecific and heterospecific gap junctional intercellular communication. *Cancer Res.* **61**, 1765–1767.
11. DeWald, D. B., Torabinejad, J., Samant, R. S., Johnston, D., Erin, N., Shope, J. C. *et al.* (2005). Metastasis suppression by breast cancer metastasis suppressor 1 involves reduction of phosphoinositide signaling in MDA-MB-435 breast carcinoma cells. *Cancer Res.* **65**, 713–717.
12. Meehan, W. J., Samant, R. S., Hopper, J. E., Carrozza, M. J., Shevde, L. A., Workman, J. L. *et al.* (2004). Breast cancer metastasis suppressor 1 (BRMS1) forms complexes with retinoblastoma-binding protein 1 (RBP1) and the mSin3 histone deacetylase complex and represses transcription. *J. Biol. Chem.* **279**, 1562–1569.
13. Cicek, M., Fukuyama, R., Welch, D. R., Sizemore, N. & Casey, G. (2005). Breast cancer metastasis suppressor 1 inhibits gene expression by targeting nuclear factor-kappaB activity. *Cancer Res.* **65**, 3586–3595.
14. Liu, Y., Smith, P. W. & Jones, D. R. (2006). Breast cancer metastasis suppressor 1 functions as a corepressor by enhancing histone deacetylase 1-mediated deacetylation of RelA/p65 and promoting apoptosis. *Mol. Cell. Biol.* **26**, 8683–8696.
15. Rivera, J., Megias, D. & Bravo, J. (2007). Proteomics-based strategy to delineate the molecular mechanisms of the metastasis suppressor gene *BRMS1*. *J. Proteome Res.* **6**, 4006–4018.
16. Samant, R. S., Clark, D. W., Fillmore, R. A., Cicek, M., Metge, B. J., Chandramouli, K. H. *et al.* (2007). Breast cancer metastasis suppressor 1 (BRMS1) inhibits

osteopontin transcription by abrogating NF-kappaB activation. *Mol. Cancer.* **6**, 6.
17. Yang, J., Zhang, B., Lin, Y., Yang, Y., Liu, X. & Lu, F. (2008). Breast cancer metastasis suppressor 1 inhibits SDF-1alpha-induced migration of non-small cell lung cancer by decreasing CXCR4 expression. *Cancer Lett.* **269**, 46–56.
18. Hurst, D. R., Xie, Y., Vaidya, K. S., Mehta, A., Moore, B. P., Accavitti-Loper, M. A. *et al.* (2008). Alterations of BRMS1–ARID4A interaction modify gene expression but still suppress metastasis in human breast cancer cells. *J. Biol. Chem.* **283**, 7438–7444.
19. Cicek, M., Fukuyama, R., Cicek, M. S., Sizemore, S., Welch, D. R., Sizemore, N. & Casey, G. (2009). BRMS1 contributes to the negative regulation of uPA gene expression through recruitment of HDAC1 to the NF-kappaB binding site of the uPA promoter. *Clin. Exp. Metastasis*, **26**, 229–237.
20. Hurst, D. R., Mehta, A., Moore, B. P., Phadke, P. A., Meehan, W. J., Accavitti, M. A. *et al.* (2006). Breast cancer metastasis suppressor 1 (BRMS1) is stabilized by the Hsp90 chaperone. *Biochem. Biophys. Res. Commun.* **348**, 1429–1435.
21. Rivera, J., Megías, D. & Bravo, J. (2010). Sorting nexin 6 interacts with breast cancer metastasis suppressor-1 and promotes transcriptional repression. *J. Cell. Biochem.* **111**, 1464–1472.
22. Schuck, P. & Rossmanith, P. (2000). Determination of the sedimentation coefficient distribution by least-squares boundary modeling. *Biopolymers*, **54**, 328–341.
23. Ward, J. J., Sodhi, J. S., McGuffin, L. J., Buxton, B. F. & Jones, D. T. (2004). Prediction and functional analysis of native disorder in proteins from the three kingdoms of life. *J. Mol. Biol.* **337**, 635–645.
24. Pollastri, G. & McLysaght, A. (2005). Porter: a new, accurate server for protein secondary structure prediction. *Bioinformatics*, **21**, 1719–1720.
25. Linding, R., Jensen, L. J., Diella, F., Bork, P., Gibson, T. J. & Russell, R. B. (2003). Protein disorder prediction: implications for structural proteomics. *Structure*, **11**, 1453–1459.
26. Shimizu, K., Hirose, S. & Noguchi, T. (2007). Poodle-s: web application for predicting protein disorder by using physicochemical features and reduced amino acid set of a position-specific scoring matrix. *Bioinformatics*, **23**, 2337–2338.
27. Berger, B., Wilson, D. B., Wolf, E., Tonchev, T., Milla, M. & Kim, P. S. (1995). Predicting coiled coils by use of pairwise residue correlations. *Proc. Natl Acad. Sci. USA*, **92**, 8259–8263.
28. Wolf, E., Kim, P. S. & Berger, B. (1997). Multicoil: a program for predicting two- and three-stranded coiled coils. *Protein Sci.* **6**, 1179–1189.
29. Lupas, A., Van Dyke, M. & Stock, J. (1991). Predicting coiled coils from protein sequences. *Science*, **252**, 1162–1164.
30. Obenauer, J. C., Cantley, L. C. & Yaffe, M. B. (2003). Scansite 2.0: proteome-wide prediction of cell signaling interactions using short sequence motifs. *Nucleic Acids Res.* **31**, 3635–3641.
31. Nakai, K. & Horton, P. (1999). PSORT: a program for detecting sorting signals in proteins and predicting their subcellular localization. *Trends Biochem. Sci.* **24**, 34–36.
32. Peri, S., Navarro, J. D., Amanchy, R., Kristiansen, T. Z., Jonnalagadda, C. K., Surendranath, V. *et al.* (2003). Development of human protein reference database as an initial platform for approaching systems biology in humans. *Genome Res.* **13**, 2363–2371.
33. Rivera, J., Megías, D., Navas, C. & Bravo, J. (2009). Identification of essential sequences for cellular localization in BRMS1 metastasis suppressor. *PLoS ONE*, **4**, e6433.
34. Lupas, A. (1996). Coiled coils: new structures and new functions. *Trends Biochem. Sci.* **21**, 375–382.
35. Mason, J. M. & Arndt, K. M. (2004). Coiled coil domains: stability, specificity, and biological implications. *ChemBioChem*, **5**, 170–176.
36. Spínola-Amilibia, M., Rivera, J. & Bravo, J. (2008). Crystallization and preliminary X-ray diffraction analysis of a breast cancer metastasis suppressor 1 predicted coiled-coil region. *Acta Crystallogr., Sect. F: Struct. Biol. Cryst. Commun.* **64**, 1156–1158.
37. McCoy, A., Grosse-Kunstleve, R., Adams, P., Winn, M., Storoni, L. & Read, R. (2007). Phaser crystallographic software. *J. Appl. Crystallogr.* **40**, 658–674.
38. Krissinel, E. & Henrick, K. (2007). Inference of macromolecular assemblies from crystalline state. *J. Mol. Biol.* **372**, 774–797.
39. Wilkins, D. K., Grimshaw, S. B., Receveur, V., Dobson, C. M., Jones, J. A. & Smith, L. J. (1999). Hydrodynamic radii of native and denatured proteins measured by pulse field gradient NMR techniques. *Biochemistry*, **38**, 16424–16431.
40. Danielsson, J., Jarvet, J., Damberg, P. & Gräslund, A. (2002). Translational diffusion measured by PFG-NMR on full length and fragments of the Alzheimer Aβ(1–40) peptide. determination of hydrodynamic radii of random coil peptides of varying length. *Magn. Reson. Chem.* **40**, S89–S97.
41. García De La Torre, J., Huertas, M. L. & Carrasco, B. (2000). Calculation of hydrodynamic properties of globular proteins from their atomic-level structure. *Biophys. J.* **78**, 719–730.
42. Lebowitz, J., Lewis, M. S. & Schuck, P. (2002). Modern analytical ultracentrifugation in protein science: a tutorial review. *Protein Sci.* **11**, 2067–2079.
43. Liu, J., Deng, Y., Dey, A. K., Moore, J. P. & Lu, M. (2009). Structure of the HIV-1 gp41 membrane-proximal ectodomain region in a putative prefusion conformation. *Biochemistry*, **48**, 2915–2923.
44. Weissenhorn, W., Dessen, A., Harrison, S. C., Skehel, J. J. & Wiley, D. C. (1997). Atomic structure of the ectodomain from HIV-1 gp41. *Nature*, **387**, 426–430.
45. Mossessova, E. & Lima, C. D. (2000). Ulp1-SUMO crystal structure and genetic analysis reveal conserved interactions and a regulatory element essential for cell growth in yeast. *Mol. Cell*, **5**, 865–876.
46. Collaborative Computational Project, Number 4. (1994). The CCP4 suite: programs for protein crystallography. *Acta Crystallogr., Sect. D: Biol. Crystallogr.* **50**, 760–763.
47. Yadav, M. K., Leman, L. J., Price, D. J., Brooks, C. L. 3., Stout, C. D. & Ghadiri, M. R. (2006). Coiled coils at the edge of configurational heterogeneity. Structural analyses of parallel and antiparallel homotetrameric coiled coils reveal configurational sensitivity to a

single solvent-exposed amino acid substitution. *Biochemistry*, **45**, 4463–4473.
48. Emsley, P. & Cowtan, K. (2004). Coot: model-building tools for molecular graphics. *Acta Crystallogr., Sect. D: Biol. Crystallogr.* **60**, 2126–2132.
49. Murshudov, G. N., Vagin, A. A. & Dodson, E. J. (1997). Refinement of macromolecular structures by the maximum-likelihood method. *Acta Crystallogr., Sect. D: Biol. Crystallogr.* **53**, 240–255.
50. Winn, M. D., Isupov, M. N. & Murshudov, G. N. (2001). Use of TLS parameters to model anisotropic displacements in macromolecular refinement. *Acta Crystallogr., Sect. D: Biol. Crystallogr.* **57**, 122–133.
51. Painter, J. & Merritt, E. A. (2006). Optimal description of a protein structure in terms of multiple groups undergoing TLS motion. *Acta Crystallogr., Sect. D: Biol. Crystallogr.* **62**, 439–450.
52. Laskowski, R. A., MacArthur, M. W., Moss, D. S. & Thornton, J. M. (1993). PROCHECK: a program to check the stereochemical quality of protein structures. *J. Appl. Crystallogr.* **26**, 283–291.
53. Davis, I. W., Leaver-Fay, A., Chen, V. B., Block, J. N., Kapral, G. J., Wang, X. *et al.* (2007). MolProbity: all-atom contacts and structure validation for proteins and nucleic acids. *Nucleic Acids Res.* **35**, W375–W383.
54. Salerno, W. J., Seaver, S. M., Armstrong, B. R. & Radhakrishnan, I. (2004). Monster: inferring non-covalent interactions in macromolecular structures from atomic coordinate data. *Nucleic Acids Res.* **32**, W566–W568.
55. Czypionka, A., de los Paños, O. R., Mateu, M. G., Barrera, F. N., Hurtado-Gómez, E., Gómez, J. *et al.* (2007). The isolated C-terminal domain of Ring1B is a dimer made of stable, well-structured monomers. *Biochemistry*, **46**, 12764–12776.
56. Schuck, P. (2000). Size-distribution analysis of macromolecules by sedimentation velocity ultracentrifugation and lamm equation modeling. *Biophys. J.* **78**, 1606–1619.
57. Schuck, P., Perugini, M. A., Gonzales, N. R., Howlett, G. J. & Schubert, D. (2002). Size-distribution analysis of proteins by analytical ultracentrifugation: strategies and application to model systems. *Biophys. J.* **82**, 1096–1111.
58. Cole, J. L. (2004). Analysis of heterogeneous interactions. *Methods Enzymol.* **384**, 212–232.